Novel three-dimensional chitosan-carbon nanotube–PVA nanocomposite hydrogel for removal of Cr6+ from wastewater

Tarek M. Eldeeb[a,b], Ahmed El Nemr[a,*], Mohamed H. Khedr[b], S.I. El-Dek[b], Neama G. Imam[c,d]

[a]Environmental Division, National Institute of Oceanography and Fisheries, Kayet Bey, El-Anfoushy, Alexandria, Egypt, emails: ahmedmoustafaelnemr@yahoo.com/ahmed.m.elnemr@gmail.com (A. El Nemr), tarikeldeeb77@yahoo.com (T.M. Eldeeb)
[b]Materials Science and Nanotechnology Department, Faculty of Postgraduates Studies for Advanced Sciences, Beni-Suef University, Beni-Suef, Egypt, emails: dkheddr@yahoo.com (M.H. Khedr), samaa@psas.bsu.edu.eg (S.I. El-Dek)
[c]Experimental Physics Department, Nuclear Research Center, Atomic Energy Authority, 13759 Cairo, Egypt, email: imam.eaea@gmail.com (N.G. Imam)
[d]Department of Chemical Physics, Chemical Center, Lund University, P.O. Box: 124, 22100 Lund, Sweden

ABSTRACT

A novel hybrid nanocomposite adsorbent was prepared by encapsulation of multi-walled carbon nano-tubes within polyvinyl alcohol/chitosan hydrogel (Cs/MWCNT/PVA) and cross-linked with glutaraldehyde. The chemical reactions between the components affected the position and intensities of the infrared bands. This nanocomposite has excellent Cr6+ ions adsorption efficiency. The optimal conditions of the process as a function of the solution pH, contact time, ionic strength, and sorbent weight were investigated. The batch equilibrium experiments revealed that the most suitable pH for chromium adsorption was at 1.5. The maximum adsorption capacity for the hydrogel was 217.4 mg g^{-1} as estimated by the Langmuir model. Other isotherm models, such as Freundlich and Temkin, were used to analyze the experimental data and the models' parameters were evaluated. The pseudo-first and second-order, Elovich, intraparticle diffusion, and film diffusion kinetic models were also investigated. The obtained results enabled to estimate the possibility to use the Cs/MWCNT/PVA hydrogel in the removal of Cr6+ ions from wastewater by adsorption.

Keywords: Cr6+ ions removal; Nanocomposite; Three-dimensional hydrogel; MWCNT; Chitosan

1. Introduction

Water, the secret of life, is the most essential element for the survival of human beings, animals, and plants on earth. Around the world, about 780 million people still lack fresh drinking water supply, especially in developing countries. This problem originates mainly from water pollution that results from human activities, such as domestic, industrial, and agricultural drainage [1,2].

Heavy metals can be distinguished from other toxic pollutants, since they are not biodegradable and can be accumulated in living tissues, causing various diseases and disorders even at very low concentrations. Some heavy metals are important for human life with relatively low concentrations but at elevated concentrations, they become harmful for humans and have different effects such as toxicity, allergenicity, carcinogenicity, and inhibition of the activity of sensitive enzymes [3]. One of these metals is chromium, which is the most abundant metal in Earth's crust, and naturally found in the environment in rocks, soil, and volcanic dust and gases. Chromium is considered one of the major industrial wastes discharged from many industries

* Corresponding author.

like tanneries, textiles, electroplating, and metallurgical which causes health issues in humans and animals and also affects marine life [4,5]. In addition, oil and coal combustion also introduce a certain amount of chromium into the environment [6].

Chromium is found in different oxidation states ranging from divalent to hexavalent, but the most stable forms are trivalent and hexavalent chromium. Chromium, which is present in zero oxidation state, is not naturally present in Earth's crust and biologically inert. Trivalent chromium has poor absorption inside the cell as compared to hexavalent chromium and trivalent chromium is proposed to be an essential nutrient for the body [7]. The most common exposure routes of chromium compounds to humans are breathing ingestion in food and water, and direct contact with skin. As shown in Table 1, many literatures investigated the removal of hexavalent chromium from aqueous solutions using different sorbents and according to the type of the sorbent and chromium concentrations, the maximum capacity of the removal varies accordingly.

General exposure to chromium takes place through emissions from industries. Chromium is used as an anti-corrosive agent in various cooling systems and combustion, for example, cigarette smoke and ash from power plants [8]. Cr^{6+} is produced by industrial processes such as electroplating, stainless steel production, leather tanning, textile manufacturing, and wood preservation. The primary health hazards caused by chromium are bronchial asthma, lung, and nasal ulcers, cancers, skin irritation, and ulceration [9], and eye irritation and damage, reproductive, and developmental problems, and is carcinogenic in nature. Other effects have been reported by Beaumont et al. [10] like indigestion, mouth ulcers, acute tubular necrosis, abdominal pain, vomiting, kidney failure, and even death when taken in excess so that in 1998 [11] has set a maximum concentration level of 100 ppb for total chromium in drinking water. According to Richard and Bourg [12], the maximum acceptable levels are reported for Cr^{3+} and Cr^{6+} ions in wastewater are 5 and 0.05 mg L^{-1}, respectively. The trivalent form of chromium apparently plays an essential role in plant and animal metabolism, while the hexavalent form is directly toxic to bacteria, plants, and animals. However, the most severe chromium compounds are chromium oxide and chromium sulfate as trivalent and chromium trioxide, chromic acid and dichromate as hexavalent chromium [13].

When the water is polluted, it must be purified; several decontamination processes of wastewater are reported in a multitude of literature such as extraction, coagulation, precipitation, evaporation, ion exchange, oxidation, biodegradation, and adsorption on carbonaceous materials [2,14–18]. Adsorption is one of the most important methods used in water purification especially for heavy metal removal from water [19–22]. Adsorption process containing appropriate adsorbent is an easy and effective process used in many applications. Adsorption is achieved by numerous kinds of adsorbent materials like fly ash and activated carbon [23].

Many synthetic and natural polymers are used as adsorbents. Modern researches focused on employing the nanomaterials as adsorbents in water purification [24–29]. Chitosan, a natural polysaccharide polymer, is considered the second abundant biopolymer beyond cellulose in nature and is characterized by the presence of primary amino groups and high nitrogen content in comparison to other natural biopolymers especially cellulose [30]. Chitosan is produced from the deacetylation of chitin extracted from two marine organisms, shrimps and crabs. Its chemical composition is a linear copolymer of D-glucosamine and N-acetyl-D-glucosamine [31]. On the other hand, chitosan has been employed for the adsorption of toxic elements, organic pollutants, and dyes [32,33]. Modification of chitosan by cross-linking with different polymers such as polyvinyl alcohol (PVA) improved its stability together with its mechanical properties. The incorporation of multiwall carbon nanotubes (CNTs) into polymers is anticipated not only to give improved thermal stability and mechanical properties but also to somewhat function as removal of organic and inorganic pollutants [34,35]. Table 1 summarizes the removal of chromium from aqueous solutions by different carbon species and its removal efficiency. The purpose of this study is to prepare a novel, three-dimensional nanocomposite hydrogel, and evaluation of its biosorption capacity for removal of hexavalent chromium ions from water.

Table 1
Comparison of different sorbents and sorption capacity for hexavalent chromium adsorption

Material used for adsorption	Capacity (mg g^{-1})	Reference
Peanut shell activated carbon	46.73	[22]
Pomegranate husk activated carbon	35.20	[18]
Guava seeds	10.50	[19]
Cross linked chitosan activated carbon	50.00	[36]
Pomegranate husk	10.59	[37]
Cross linked xanthated chitosan	625.00	[38]
Kapok fiber	110.13	[39]
Chitosan cross-linked poly alginic acid	26.49	[40]
Green alga activated carbon	112.36	[41]
Casuarina activated carbon	172.40	[16]
Date palm seed activated carbon	120.48	[18]
Cs/MWCNT/PVA nanocomposite	217.00	This study

In addition, the kinetics and reaction mechanisms of adsorption were investigated.

2. Materials and methods

2.1. Chemicals

Multi-walled carbon nanotubes (MWCNT) were prepared by chemical vapour deposition (CVD) method, using a tube furnace, with a 45 mm diameter and 60 cm length quartz tube. PVA (MW: 30,000–70,000) was purchased from Sigma-Aldrich. Chitosan polymer (degree of deacetylation 93.0%, MW: 161.16) was acquired from Oxford India. Acetic acid anhydride and ethyl alcohol were obtained from ADWIC, Egypt. Hydrochloric acid 32%, ethanol 95%, and glutaraldehyde 50% were purchased from El Nasr Pharmaceutical Chemicals Co., Egypt. All chemicals were used without further purification. Fig. 1 represents the flow chart of the preparation of three-dimensional hydrogel and batch experiments.

2.2. Preparation of Fe/Co/CaCO₃ supporting catalyst

The supporting catalyst for MWCNT production was prepared according to the method reported by Schwarz [42] when an appropriate quantity of calcium carbonate was milled in a ball mill for about 12 h to minimize the particle size and increase the surface area, then calcium carbonate, ferric nitrate $Fe(NO_3)_3 \cdot 9H_2O$, and cobalt nitrate $Co(NO_3)_2 \cdot 6H_2O$ were mixed with definite ratios of 95%, 2.5%, and 2.5%, respectively. The mixture was then milled again for 2 h, after that, it was made in the form of a paste by adding a small amount of distilled water and mixed well homogenously, dried at 120°C overnight, and then ground to get fine powder of supporting catalyst [43].

2.3. Preparation of MWCNT

The chemical vapor deposition method was used for the synthesis of MWCNT, in which acetylene with iron and cobalt mixture in an inert gas atmosphere was introduced into the reaction chamber. During which, nanotubes were formed on the substrate by the decomposition of the hydrocarbon at a temperature of 600°C–900°C at atmospheric pressure. The dimensions of the produced nanotubes are related to the size of the metal particle used. This technique offers more control over the length and structure of the produced nanotubes compared with arc and laser methods.

This process can also be scaled up to produce industrial quantities of MWCNT. According to the method reported by [43], MWCNT were prepared as follows: 2.0 g of the supporting catalyst was placed in alumina boat and introduced into the cylindrical quartz tube fitted inside a tube furnace and adjusted at 600°C and the catalyst was preheated for 10 min in the presence of nitrogen gas flow by a rate of 90 mL min⁻¹. After catalyst heating, a flow of acetylene gas was allowed to pass over the catalyst through the quartz tube at a flow rate of 90 mL min⁻¹ for 40 min. After the desired time, acetylene flow was stopped and the product was cooled to room temperature.

2.4. Purification and functionalization of MWCNT

The extremely large surface area leads to a strong tendency to form agglomerates. Surface functionalization helps in stabilizing the dispersion since it can prevent reaggregation of nanotubes and also leads to the coupling of MWCNT with a polymeric matrix. Covalent functionalization of MWCNT can be achieved by introducing some functional groups on defect sites of MWCNT by using oxidizing agents such as strong acids, which results in the formation of carboxylic or hydroxyl groups (–COOH, –OH) on the surface of nanotubes. This type of functionalization is known as defect group functionalization [43]. The functionalization process was performed as follows: Typically, 30 mL of concentrated HNO_3 and 10 mL of concentrated H_2SO_4 were injected into a 250 mL flask loaded with 5 g phosphorus pentoxide and 10 g of as obtained MWCNT. The mixture was refluxed at 350°C for 2 h to obtain the MWCNT suspension solution.
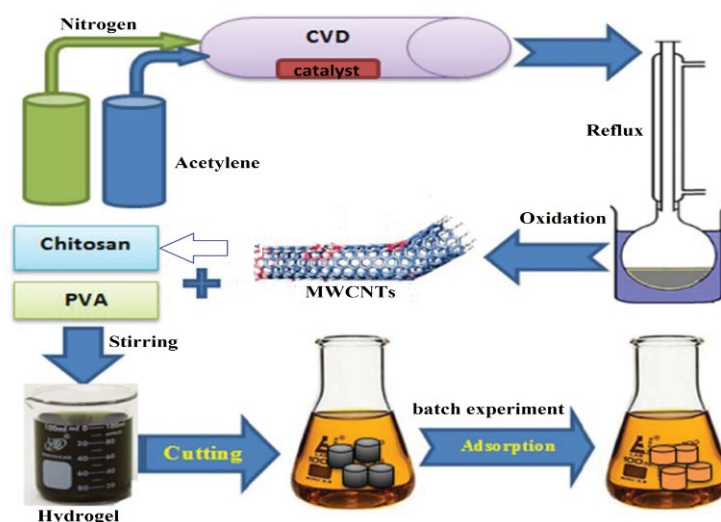

Fig. 1. Flow chart of preparation and batch experiments.

The solution was washed with deionized water until the pH of the filtrate approached that of distilled water. The final step was drying at 50°C overnight to obtain carboxylated MWCNT (MWCNT–COOH).

2.5. Preparation of three-dimensional hydrogel composite

The solution of PVA was prepared by dissolving PVA (20 wt.% W/V) in distilled water for 2 h at 95°C with constant stirring until a transparent homogenous solution was created. Then, chitosan solution was prepared by dissolving chitosan powder (4 wt.% W/V) in 2% acidified distilled water with glacial acetic acid under continuous vigorous magnetic stirring at room temperature till the viscous liquid solution was formed. The hydrogel was prepared by dispersion of MWCNT in the aqueous solution of PVA using an ultrasonic water bath and magnetic stirrer followed by mixing with chitosan solution and finally cross-linking. An appropriate amount of MWCNT was added to about 35 g of PVA solution and the mixture was magnetically stirred for 5 min followed by sonication in water-bath sonicator for about 10 min then an equal amount of chitosan was added to the mixture and stirred for 10 min, keeping the beaker at room temperature. Then, 0.5 mL of 50% glutaraldehyde as a cross-linker and three drops of 34% HCl as a catalyst were added to the previous mixture with continuous stirring.

2.6. Preparation of synthetic standard solution of metal

All used chemicals were of analytical grade, and the adsorption experiments were carried out at room temperature (25°C ± 2°C). 1,000 ppm stock solution of Cr^{6+} was prepared by dissolving 2.834 g of $K_2Cr_2O_7$ in 1,000 mL of double distilled water in a measuring flask. Before performing the batch experiments, the initial pH of each chromium concentration solution was adjusted at pH 1.5 with 0.1 M HCl or 0.1 M NaOH. The concentrations of free Cr^{6+} ions in the stock solution and unadsorbed chromium ions in the adsorption medium was determined by spectrophotometer at λ 540 nm using 100 ppm diphenylcarbazide, which gives a red-violet colored complex [16–18].

2.7. Measurements and characterization

Fourier transform infrared spectroscopy (FTIR) spectrum was carried out using Bruker Model Vertex 70 FTIR spectrometer, Germany, with a range of 3,600–500 cm^{-1} connected to Platinum ATR unit, Bruker, Germany. Brunauer–Emmett–Teller (BET) adsorption–desorption experiments were carried out on BELSORP-mini II, BEL Japan, Inc. The specific surface area, mean pore diameter, pore-volume, and mean particle size of the pristine and oxidized MWCNT were determined using N_2 adsorption–desorption measurements at liquid nitrogen temperature 77 K as adsorption temperature and 89.62 kPa saturated vapor pressure. All procedures including sample preparation, dispersion, and analysis were carried out according to the manual guide of the instrument. Field emission scanning electron microscopy micrographs were taken using scanning electron microscopy (SEM) Model Quanta 250 FEG (field emission gun), with

accelerating voltage 30 kV FEI Company, The Netherlands. Transmission electron microscopy (TEM) micrographs were taken by TEM model TECNAI SPIRIT 120 kV, FEI Company, The Netherlands. X-ray diffraction (XRD) analysis was carried out by PANalytical. The scanning range was 10°–90° using Cu Kα, radiation. The residual chromium concentration was measured [37] using a UV-vis spectrophotometer (Analytik Jena, SPEKOL 1300, Germany) using a quartz cell of path length 1.0 cm at wavelength λ 540 nm.

3. Results and discussion

3.1. Spectral, structural, and microstructure analysis

3.1.1. FTIR spectra

FTIR spectra of functionalized MWCNT, pure PVA, pure chitosan and Cs/MWCNT/PVA nanocomposite are represented in Fig. 2 and Table 2. In the spectrum of functionalized MWCNT (Fig. 2a), the bands at 3,304 and 3,075 cm^{-1} are identified as O–H stretching of carboxylic group and N–H stretching, respectively. The bands around 2,966 and 2,668 cm^{-1} are due to SP^3 aliphatic C–H, in addition, the presence of two bands at 1,659 and 1,496 cm^{-1} are ascribed to C=O of the carboxylic group [44]. Fig. 2b represents the adsorption spectra of PVA, the broad and strong bands at 3,292 cm^{-1} is assigned to stretching vibration of O–H and hydrogen bonding another absorption band at 2,921 cm^{-1} was attributed to stretching absorption of C–H, in addition to the peaks at 1,426; 1,246; and 1,084 cm^{-1} which are corresponding to the adsorption peaks due to stretching vibration absorption of the CH$_2$ and stretching band of C–O, respectively [45,46]. In the spectra of chitosan (Fig. 2c), there is an overlapping between N–H and O–H stretching vibrations as a proud band around 3,355 cm^{-1}, which represents the amino and hydroxyl groups. The peaks at 1,023; 1,373; 1,590; and 1,647 cm^{-1} was assigned to the C–O stretching vibration of the CH$_2$OH and primary alcoholic group [44,47–49] and the N–H bending of NH$_2$ and N–H stretching vibration, respectively [48]. The change in the characteristic spectrum of the Cs/MWCNT/PVA nanocomposite (Fig. 2d) as well as shifting of the band at 1,647 to 1,640 cm^{-1} indicated the hydrogen bonding formation between functional groups of modified MWCNT and NH$_2$ as well as OH groups of Cs and PVA [26].

3.1.2. Morphology and microstructure investigation

Scanning, transmission, and high-resolution transmission electron microscopy (HR-TEM) are useful tools to study the surface morphology of the CNTs and enable us to follow up on the removal of the impurities such as the catalyst metal particles and amorphous carbon moieties from as prepared MWCNT [50]. Figs. 3a and b show the SEM images of unpurified and functionalized MWCNT, respectively.

The presence of the metal particles and amorphous carbon in the untreated sample and disappearance of the impurities after acid treatment and the absence of any evidence of tubular shape damage. This observation is confirmed through the TEM image (Fig. 4a) that ensured there are no changes occurred in the walls of MWCNT and also the removal of amorphous carbon impurities and metal clusters [51]. TEM micrograph (Fig. 4a) proved that the tubular
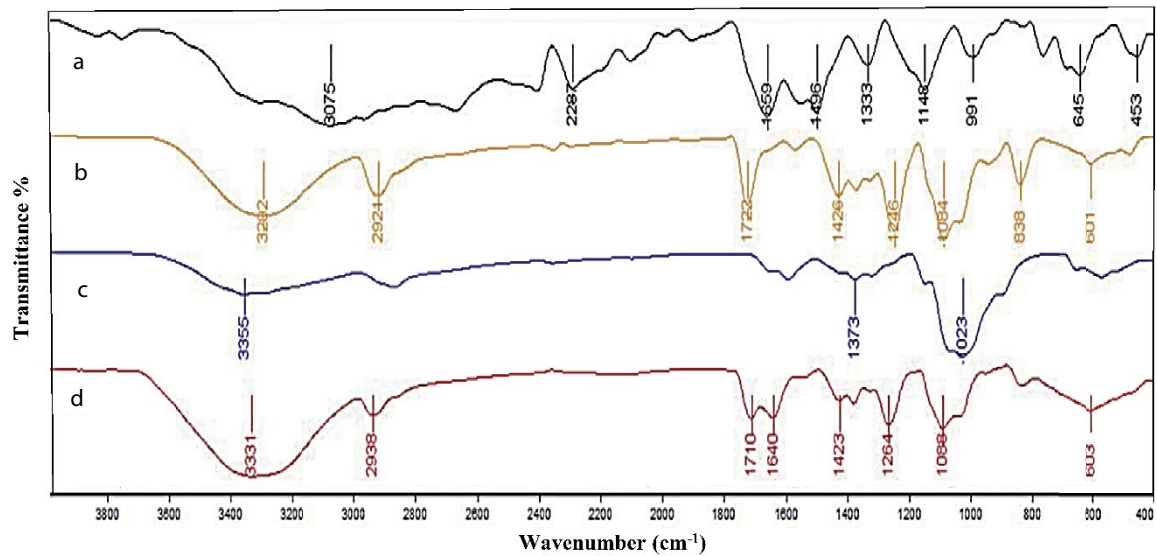
Fig. 2. FTIR spectrum of oxidized MWCNT (a), pure PVA (b), pure chitosan (c), and Cs/MWCNT/PVA hydrogel (d).
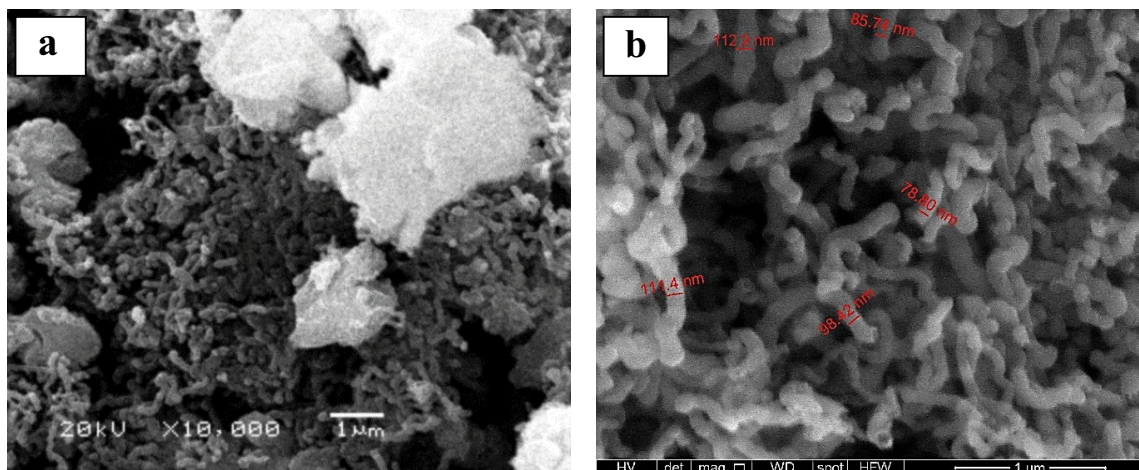

Fig. 3. Field emission-scanning electron microscopy (FE-SEM) image of (a) unpurified MWCNT and (b) functionalized MWCNT.

diameter ranged from 78 to 112 nm and the wall thickness is ranged from 8 to 10 nm. HR-TEM micrograph of purified MWCNT illustrated in Fig. 4b showed the clear appearance of the multiwall structure of the CNTs and the end caps are still closed and not affected by the acid purification. Scan micrograph of the prepared nanocomposite as shown in Figs. 4c and d improve the good dispersion of MWCNTs throughout the mixture of the hydrogel giving better mechanical properties. We conclude the tubular structure of MWCNT is clear and preserved. These results are supported by XRD analysis.

3.1.3. XRD analysis

Fig. 5 represents the XRD pattern of pristine and acid-purified MWCNT. The pristine MWCNT has no distinct, strong diffraction peaks indicating the amorphous nature. For the oxidized MWCNT, there are two strong peaks at 2θ at 26.02° and 41.82° that are related to graphite structure (002)

and (100) planes of purified MWCNT which provides the enhanced crystallinity and decreases the amorphous nature as a result of acid treatment [26,52,44].

3.1.4. BET surface analysis

Nitrogen adsorption–desorption study and BET analysis technique was used to measure pore diameter and specific surface area of MWCNT. The results of the BET surface area analysis of MWCNT show that the total surface area is 182 m^2 g^{-1} and the pore diameter is 6.7 nm. It was observed that the MWCNT has a less specific surface area than that distinguished by [26].

3.2. Bach experimental study

At equilibrium, the adsorbed amount of Cr^{6+} onto MWCNT composite hydrogel q_e (mg g^{-1}) was determined according to the following mass balance Eq. (1):
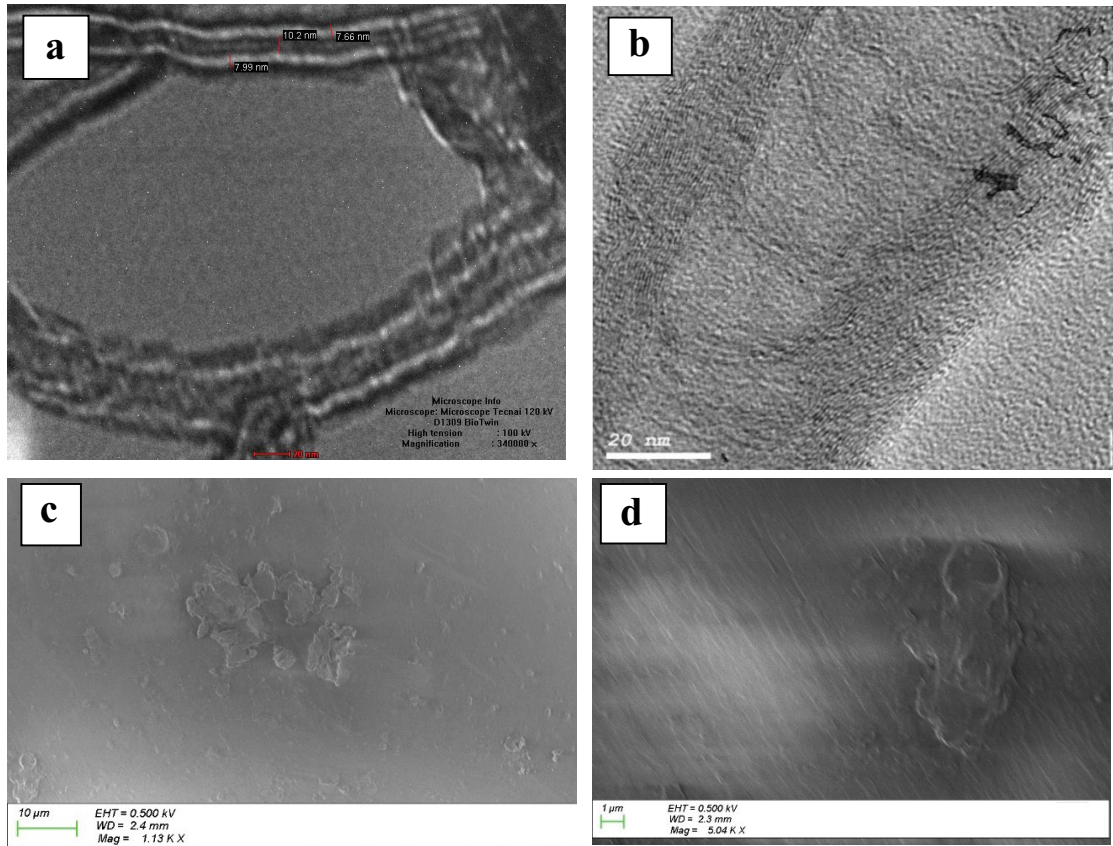
Fig. 4. (a) TEM and (b) HR-TEM images of oxidized-purified MWCNT (c,d) SEM images of the prepared nanocomposite.
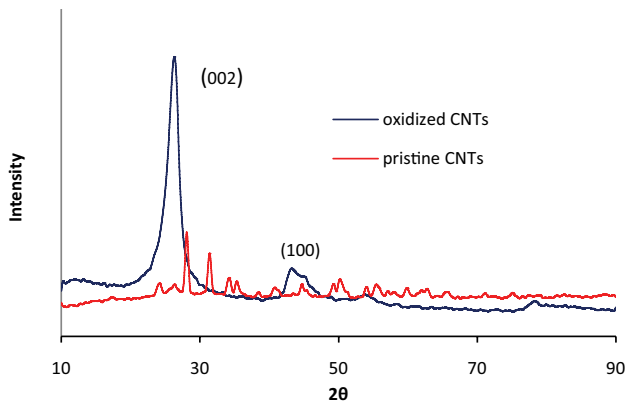

Fig. 5. XRD pattern of pristine and oxidized MWCNT.

$$q_e = \frac{(C_0 - C_e) \times V}{W} \qquad (1)$$

where C_0 and C_e are the initial and equilibrium liquid-phase concentrations of Cr^{6+}, respectively (mg L^{-1}), V is the volume of the solution in a liter, and W is the weight of the used MWCNT in g L^{-1}. The amount of adsorbed Cr^{6+} adsorbed at time t was calculated by the following equation:

$$q_t = \frac{(C_0 - C_t) \times V}{W} \qquad (2)$$

where C_0 and C_t are the concentrations of Cr^{6+} (mg L^{-1}) at initial and given time t, respectively, V is the volume of the solution in a liter, and W is the weight of the used MWCNT in g L^{-1}. However, the removal efficiency ($R\%$) of Cr^{6+} from the aqueous phase by adsorption on MWCNT hydrogel surface was calculated by the following Eq. (3):

$$R\% = \frac{(C_0 - C_t)}{C_0} \times 100 \qquad (3)$$

where C_0 and C_t are the liquid-phase concentrations of Cr^{6+} at initial and given time t (mg L^{-1}), respectively.

3.2.1. Effect of pH on metal adsorption

According to the previous studies on the adsorption of heavy metals, pH is the most effective factor in the adsorption process [16–18,37,41]. To determine the optimum pH condition on the Cr^{6+} removal by MWCNT composite hydrogel, experiments were carried out at different pH values (1.5, 3, 5, and 7) using 150 ppm initial concentration of Cr^{+6} solution and 1.5 g L^{-1} of the composite hydrogel. The suspensions were shaken at room temperature (25°C ± 2°C) at 200 rpm for 2 h and the amount of chromium adsorbed was determined [37]. The efficiency of composite on chromium uptake at different pH is represented in Fig. 6. All the experiments are duplicated and only the mean values are reported. The maximum deviation observed was less than ±5%.

Table 2
FTIR band assignment

Materials	Wavenumber (cm^{-1})	Assignment
	3,304	O–H stretching of COOH
	3,075	N–H stretching
MWCNT	1,659	C=O stretching of COOH
	2,966–2,668	Sp^3 aliphatic C–H
	1,333–1,549	–NH$_2$
	3,292	O–H stretching vibration
PVA	2,921	C–H stretching band
	1,426	CH$_2$ stretching vibration
	1,246–1,084	C–O stretching vibration
	3,355	Overlapping of stretching O–H and N–H
	1,590	–NH$_2$ bending
Chitosan	1,647	Amid-I
	1,373	Amid-III
	1,023	Skeletal vibration involving C–O–C
Chitosan/MWCNT/PVA	3,331	Overlapping of stretching O–H and N–H
nanocomposite	2,938	C–H stretching
	1,640	C=O stretching of acetyl group

As observed in Fig. 6, the higher uptake value was observed at pH 1.5 and then decreased significantly with increasing pH till it reached the lowest removal value at pH 7. This is attributed to the fact that the adsorption capacity is highly pH-dependent and the adsorption mechanism is depending on composite surface charge and the chromium ion species in the solution. At optimum adsorption pH ≈ 1.5, the dominant species of Cr^{6+} ions in solution are $HCrO_4^-$, $Cr_2O_7^{2-}$, $Cr_4O_{13}^{2-}$ and $Cr_3O_{10}^{2-}$, which could be adsorbed primarily by electrostatically attraction [53]. In the same time at very low pH values, the adsorbent surface surrounded by the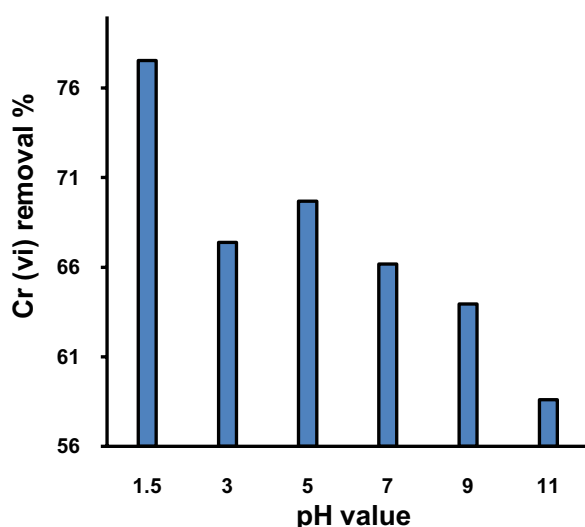 hydronium ions which enhance the Cr^{6+} interaction with binding sites of the hydrogel by attraction forces by increasing pH values $HCrO_4^-$ is shifted to form $Cr_2O_7^-$ and CrO_4^{2-} and will preferably exist in the solution which are less adsorbed to the sorbent surface [54,55], and the overall surface charge on the hydrogel became negatively charged and the repulsive forces act to decrease the adsorption of chromium ions [56]. Also, it has been known that in the case of high chromium concentration, the $Cr_2O_7^{2-}$ ions precipitate at higher pH values. On the other hand, at the high pH values, the surface of the composite became highly protonated due to surrounding hydronium ions that favored the interaction of the Cr^{6+} ion with binding sites of composite by greater attractive forces.

Increasing concentration of hydronium ions surrounding the sorbent particles surfaces, which lowers the net positive surface potential of the sorbent. This reduces the attractive forces between adsorbent and adsorbate. In addition, as the pH moved toward the basic value, the sorbent surface possesses more negatively charged functional groups. There exists a competition between two negatively charged anions, OH$^-$ and the metal cations. Moreover, in the alkaline solution (pH above 8), the predominant species is CrO_4^{2-} and in case of a high concentration of chromium ion, the $Cr_2O_7^{2-}$ ions were precipitated [57].

3.2.2. Effect of adsorption time

Fig. 7 shows the effect of adsorption time using Cs/MWCNT/PVA hydrogel (containing 0.3 L^{-1} of MWCNT) at pH 1.5. From the graph, we remarked that the rate of chromium adsorption on the Cs/MWCNT/PVA hydrogel rises sharply in the first 10 min. After that, it increases gradually till reaches 60%–80% removal in a period of 1 h and finally rises slowly to reach near the equilibrium at 2 h with removal efficiency ranged from 71% to 88% according to the initial
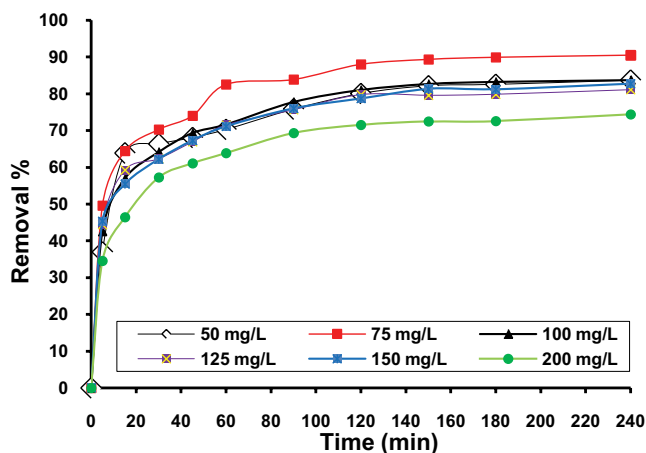

Fig. 6. Effect of pH on the adsorption of Cr^{6+} (150 ppm) on the Cs/MWCNT/PVA hydrogel (1.5 g L^{-1}) at 25°C ± 2°C.

Fig. 7. Effect of contact time on the removal of different initial concentrations of Cr^{6+} ions using the Cs/MWCNT/PVA hydrogel (containing 0.3 g L^{-1} of MWCNT) at pH 1.5.

concentration of hexavalent chromium ions. Then increasing the contact time to 4 h leads to a slight increase in the removal percentage to be between 75% and 91%. As the initial concentration of chromium ions increases, the removal rate decreased which was an obvious result.

3.2.3. Adsorption isotherm

Adsorption isotherm batches were carried out at room temperature, by agitating 250 mL conical flasks containing hydrogel (containing 0.1, 0.2, 0.3, 0.4, 0.5, and 0.6 g L^{-1} of MWCNT) that were thoroughly mixed with 100 mL of chromium solutions on a shaker for 3 h. The isotherm studies were performed by varying the initial chromium concentrations (50, 75, 100, 125, 150, and 200 mg L^{-1}) at pH 1.5. The pH value was adjusted using 0.1 M HCl or 0.1 M NaOH before the addition of biomass and was maintained throughout the experiment.

3.2.3.1. Langmuir adsorption isotherm investigation

The Langmuir non-linear equation may be written as Eq. (4):

$$q_e = \frac{Q_m K_a C_e}{1 + K_a C_e} \tag{4}$$

where Q_m is a constant that reflects a complete monolayer capacity (maximum capacity, mg g^{-1}) and K_a is the adsorption equilibrium constant (L mg^{-1}) that is related to the apparent energy of sorption and can be employed as indicator of isotherm rise in the region of lower residual metal concentration, which reflects the affinity or strength of the adsorbent for the adsorbate [58,59]. The Langmuir Eq. (4) can be linearized as shown in Eq. (5), which gives different ways for parameter estimation [60,61]. The values of Q_m and K_a obtained from plot of C_e against C_e/Q_e (Fig. 8a) are presented in Table 3. We can conclude that the Langmuir isotherm model can't be fitted to the adsorption process because the correlation coefficient (R^2) is less than 0.95.

$$\frac{C_e}{Q_e} = \frac{1}{K_a Q_m} + \frac{1}{Q_m} \times C_e \tag{5}$$

3.2.3.2. Freundlich isotherm investigation

In 1906, Freundlich [62] postulated the earliest isotherm model to describe the adsorption process and formulated its non-linear equation as Eq. (6):

$$q_e = K_f C_e^{1/n} \tag{6}$$

where K_f (mg g^{-1}) is the Freundlich constant which is related to the relative adsorption intensity of the metal ions on the adsorbent. It can be defined as a distribution or adsorption coefficient that represents the number of chromium ions adsorbed onto the hydrogel surface for unit equilibrium concentration. $1/n$ is a constant which indicates the adsorption capacity of the chromium ions onto the hydrogel or surface heterogeneity. n is called heterogeneity factor which represents the deviation from linearity of adsorption as follows: when $1/n$ is equal to 1, the adsorption is linear and the metal ion concentration doesn't affect the partition between two phases. In the case of $1/n$ is less than 1, there is chemical adsorption and this indicates a normal Langmuir isotherm, but when $1/n$ is more than 1, cooperative adsorption and the adsorption is more favorable physically and involves strong interactions between the molecules of the adsorbate [63,64]. Also, the exponential expression of the Freundlich equation assumes that the concentration of the adsorbate on the surface of the adsorbent increases as the adsorbate concentration increases. The linearized form of the Freundlich equation is shown as Eq. (7).

$$\log q_e = \log K_f + \frac{1}{n} \log C_e \tag{7}$$

From the linearized form, we can conclude that there is a logarithmic decrease in the enthalpy of sorption with the increase in the fraction of the occupied sites. The plot of the linear Freundlich isotherm for the adsorption of the chromium onto Cs/MWCNT/PVA hydrogel is represented in Fig. 8b. The correlation coefficients given in Table 3 concluded that the Freundlich isotherm is more applicable than the Langmuir model since the correlation coefficient ranged between 0.96 and 0.99. The value of $1/n$ is less than 1, showing that only one mechanism has taken place and ensure that the experimental data is in good agreement with the Freundlich model and the adsorption of chromium ions onto Cs/MWCNT/PVA is a physical process.

3.2.3.3. Temkin model

In 1940, Temkin and Pyzhev [65] presented a new theory for the interpretation of the adsorption process depending on the consideration of the indirect effects of the adsorbate–adsorbate interactions. Temkin assumes that the heat of adsorption of all molecules on the surface layer of the adsorbent species decreases linearly with increasing adsorbate covering layer due to indirect adsorbate–adsorbate repulsions, and the adsorption is a uniform distribution of

Table 3
Comparison of the coefficients isotherm models for Cr^{6+} adsorption onto Cs/MWCNT/PVA hydrogel

Isotherm model	Isotherm parameter	MWCNT concentrations (g L^{-1})					
		0.10	0.20	0.30	0.40	0.50	0.60
Freundlich	$1/n$	0.52	0.56	0.40	0.59	0.58	0.61
	K_F (mg$^{1-1/n}$ L$^{1/n}$ g^{-1})	20.38	8.46	6.05	7.74	3.25	2.49
	R^2	0.99	1.00	0.98	0.99	0.98	0.96
Langmuir	Q_m (mg g^{-1})	217.39	111.11	75.19	47.39	47.39	40.32
	$K_a \times 10^3$	90.00	57.00	62.00	69.00	43.00	33.00
	R^2	0.95	0.98	0.86	0.91	0.98	0.87
Temkin	A	0.493	0.381	0.398	0.377	0.359	0.331
	B	45.60	24.23	16.33	12.62	10.13	8.80
	R^2	0.95	0.97	0.90	0.99	0.99	0.93
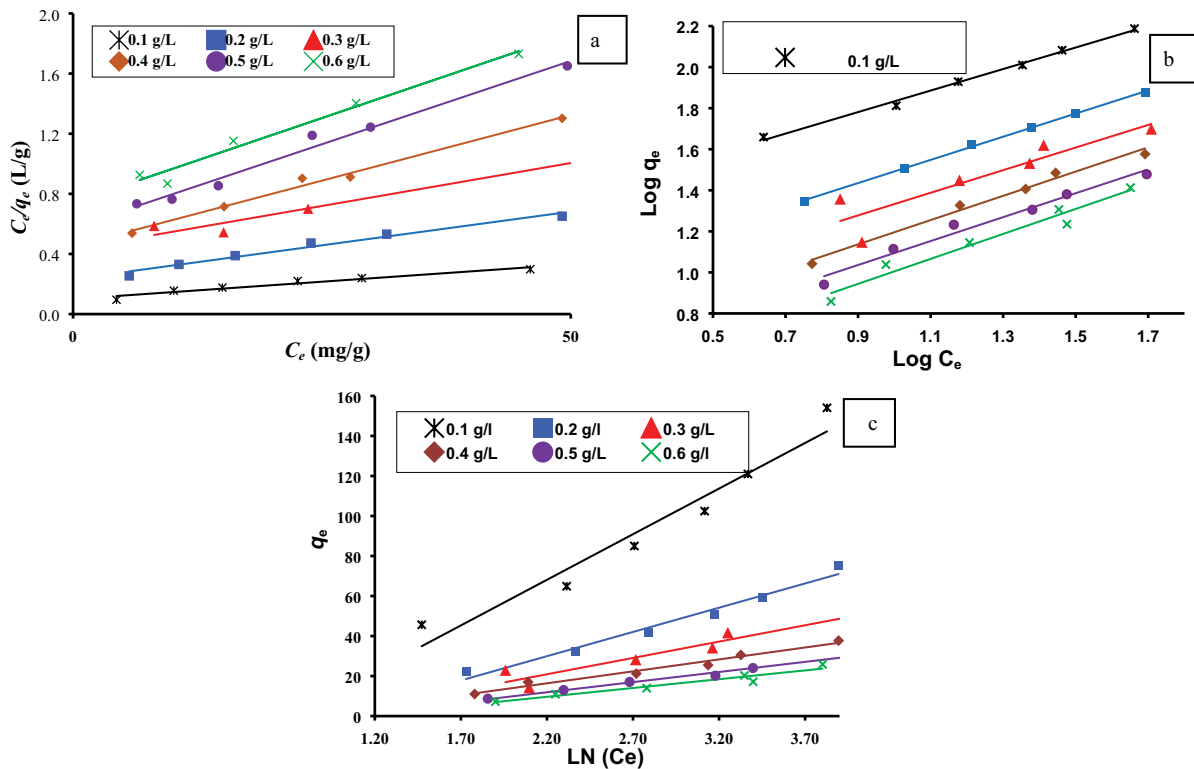
Fig. 8. (a) Linear Langmuir, (b) Freundlich, and (c) Temkin isotherms of Cr^{6+} (50–200 mg L^{-1}) adsorbed onto Cs/MWCNT/PVA hydrogel (0.1–0.6 g L^{-1}).

uniform maximum binding energy [66,61]. Inversely with the Freundlich equation, Temkin considered that the lowering in the heat of adsorption is linear rather than logarithmic and he formulated his results in the following equations:

Non-linear form Eq. (8):

$$q_e = \frac{RT}{b}\ln(AC_e) \tag{8}$$

Linear form Eq. (9):

$$q_e = B\ln A + B\ln C_e \tag{9}$$

where $B = (RT/b)$ is Temkin constant and related to the heat of sorption, since T is the absolute temperature in Kelvin and R is the universal gas constant, 8.314 J mol^{-1} K^{-1}. A is the equilibrium binding constant (L min^{-1}) related to the maximum binding energy [67]. Plotting q_e vs. lnC_e according to Eq. (9) enables us to determinate the isotherm constants A and b (Fig. 8c). The isotherm parameters obtained from Temkin models are reported in Table 3. From the data analysis, we can conclude that the correlation coefficient obtained $R^2 \leq 97$, which indicates that Temkin isotherm is less applicable than Langmuir's and Freundlich's isotherm models.

3.2.4. Kinetics studies

Kinetic studies were performed at pH 1.5 by mixing of hydrogel (containing 0.1, 0.2, 0.3, 0.4, 0.5, and 0.6 g L^{-1} of MWCNT) with 100 mL of Cr^{6+} solution (50, 75, 100, 125, 150, and 200 mg L^{-1}) and agitated at speed of 200 rpm for 180 min at room temperature. Samples of 0.5 ml were collected from the duplicate flasks at different time intervals (5, 15, 30, 45, 60, 90, 120, 150, and 180 min) and analyzed for residual Cr^{6+} in the solution. The kinetic parameters are employed to explore the adsorption rate and provide important data for modeling and designation of the optimum operating conditions for a full-scale batch process. Moreover, the kinetic studies reveal the process by which the metal removed from the aqueous phase by a certain adsorbent.

To understand the dynamics of the adsorption of Cr^{6+} on the hydrogel in terms of the order of the rate constant, the kinetics of the reaction should be studied. Several models were investigated to evaluate the rate-controlling steps of the adsorption process such as chemical reaction, diffusion control, and mass transfer. The pseudo-first-order [68,69] and pseudo-second-order [70] kinetic models were employed for Cr^{6+} ions adsorption on the hydrogel. The correlation coefficient (R^2) was measured and the higher value of R^2 is, the more applicable model to the kinetics of Cr^{6+} adsorption.

3.2.4.1. Pseudo-first-order kinetic model

In 1898 Lagergren [69] has reported the first known kinetic model used for the description of the rate of the adsorption of certain adsorbate on the surface of adsorbent depending on the adsorption capacity, and he formulated his theory in the following equation:

$$\frac{dq_t}{d_t} = k_1\left(q_e - q_t\right) \tag{10}$$

By integrating Eq. (10) for the boundary conditions $t = 0$ to $t = t$ and $q_t = 0$ to $q_t = q_t$ gives Eq. (11):

$$\log\left(\frac{q_e}{q_e - q_t}\right) = \frac{k_1}{2.303}t \tag{11}$$

Eq. (11) can be rearranged to give the linear form of the integrated rate low of pseudo-first-order kinetic model:

$$\log\left(q_e - q_t\right) = \log\left(q_e\right) - \frac{k_1}{2.303}t \tag{12}$$

where q_e and q_t are the amounts of Cr^{6+} (mg g^{-1}) at equilibrium and time t, respectively, and k_1 is the equilibrium rate constant of pseudo-first-order adsorption (L min^{-1}). From the plot of log(q_e–q_t) vs. t, we can calculate the values of the rate constant k_1, equilibrium adsorption capacity q_t, and the correlation coefficient. The data obtained from the batch experiments are given in (Fig. 9a) and Table 4. The correlation coefficients R^2 are found to be high but in comparison to that of the pseudo-second-order reaction, they are significantly low. In addition, there is no agreement between calculated q_e and experimental q_e. Indeed, we can conclude

that the adsorption of Cr^{6+} onto Cs/MWCNT/PVA hydrogel doesn't imply the pseudo-first-order reaction.

3.2.4.2. Pseudo-second-order kinetic model

Pseudo-second-order kinetic model was postulated by Ho et al. [70] and formulated his theory in the following equation:

$$\frac{dq_t}{d_t} = k_2\left(q_e - q_t\right)^2 \tag{13}$$

By the integration of the last equation for the boundary conditions $t = 0$ to $t = t$ and $q_t = 0$ to $q_t = q_t$ and simplified to give the linear form of Eq. (14):

$$\left(\frac{t}{q_t}\right) = \frac{1}{k_2 q_e^2} + \frac{1}{q_e}\left(t\right) \tag{14}$$

where q_e is the equilibrium adsorption capacity and k_2 (g mg^{-1} min^{-1}) is the second-order rate constant of adsorption and was used to obtain the initial adsorption rate h (mg g^{-1} min^{-1}) through Eq. (15).

$$h = k_2 q_e^2 \tag{15}$$

If plotting (t/q_t) vs. t gives a linear relationship, the pseudo-second-order model will become applicable; from the linear relationship, we can obtain the values of q_e and k_2 from the slope and intercept of the linear line, respectively. Applying pseudo-second-order kinetic model to our experimental data as expressed in Fig. 9b and Table 4 we found that there is a good agreement between the pseudo-second-order model for the adsorption of Cr^{6+} on Cs/MWCNT/PVA hydrogel, in addition to the correlation coefficient (R^2) $\geq$ 0.99. Also, it was found that the calculated equilibrium adsorption capacity q_e values were very close to the experimental data. Moreover, the initial adsorption rate values (h) were found to be increased by increasing the initial chromium concentrations.

Inversely, the second-order rate constant k_2 values were inversely proportional to the initial chromium concentrations from 50 to 200 mg L^{-1} as shown in Table 4.

From the previous discussion, we conclude that the chromium adsorption from aqueous solution on Cs/MWCNT/PVA hydrogel obeys the second-order kinetic isotherm.

3.2.4.3. Elovich kinetic model

Another determining rate equation depending on the adsorption capacity is Elovich equation which expressed as follow [71–73]:

$$q_t = \frac{1}{\beta}\ln\left(\alpha\beta\right) + \frac{1}{\beta}\ln\left(t\right) \tag{16}$$

where α represents the initial adsorption rate (mg g^{-1} min^{-1}) and β represents the desorption constant (g mg^{-1}). By plotting q_t vs. ln(t) as in Fig. 9c we obtain a straight line with intercept and slop from which we can obtain the constants α and β

Table 4
Comparison of the pseudo-first and second-order adsorption rate constants and calculated and experimental q_e values for different initial Cr^{6+} and carbon nanotube concentrations

Parameter			First-order kinetic model			Second-order kinetic model			
CNTs conc.	Cr^{+6} (mg L^{-1})	q_e (exp.)	q_e (calc.)	$k_1 \times 10^3$	R^2	q_e (calc.)	$k_2 \times 10^3$	h	R^2
	50	45.64	37.08	36.39	0.845	46.95	2.52	5.55	0.999
	75	64.88	33.62	22.34	0.988	67.57	0.69	3.15	0.999
0.1 g L^{-1}	100	85.00	43.66	21.42	0.965	88.50	0.38	2.99	0.999
	125	102.44	58.33	23.49	0.988	107.53	0.35	4.02	0.999
	150	120.99	141.80	36.85	0.837	126.58	0.36	5.71	0.999
	200	154.07	252.64	41.91	0.764	161.29	0.22	5.71	0.999
	50	22.18	7.34	17.73	0.940	22.68	6.41	3.30	1.000
	75	32.18	15.62	26.25	0.978	33.22	3.97	4.39	0.999
0.2 g L^{-1}	100	41.86	17.96	18.65	0.986	43.29	2.54	4.76	1.000
	125	50.55	29.09	24.87	0.978	52.63	1.91	5.30	0.999
	150	59.24	70.36	38.00	0.906	61.73	1.55	5.90	0.999
	200	75.44	64.15	31.32	0.847	78.13	1.42	8.69	1.000
	50	13.95	6.33	20.04	0.969	14.43	7.29	1.52	0.999
	75	22.64	14.58	29.25	0.946	23.42	5.21	2.86	0.999
0.3 g L^{-1}	100	27.91	22.31	31.32	0.934	28.99	3.70	3.11	0.999
	125	33.80	25.77	32.01	0.857	34.84	3.52	4.28	0.999
	150	41.40	34.28	30.40	0.904	42.92	3.20	5.90	0.999
	200	49.63	21.81	18.19	0.963	51.28	1.97	5.18	1.000
	50	11.02	7.16	29.71	0.962	11.38	11.44	1.48	1.000
	75	17.79	11.27	24.41	0.984	18.76	4.29	1.51	0.998
0.4 g L^{-1}	100	21.22	17.00	33.85	0.855	21.98	5.22	2.52	0.999
	125	25.49	7.27	14.74	0.914	26.32	5.04	3.49	0.999
	150	30.54	31.88	31.78	0.849	31.75	3.06	3.09	0.999
	200	37.72	33.20	35.01	0.944	39.22	2.84	4.37	0.999
	50	8.72	3.93	27.64	0.989	8.98	17.23	1.39	1.000
	75	13.01	6.60	20.27	0.986	13.51	6.96	1.27	0.998
0.5 g L^{-1}	100	17.08	8.07	23.49	0.934	17.57	7.16	2.21	0.999
	125	20.20	17.46	32.93	0.917	21.01	4.97	2.19	0.999
	150	24.02	11.77	21.19	0.985	24.94	4.14	2.57	0.999
	200	30.07	12.11	16.58	0.934	31.35	3.37	3.31	0.999
	50	7.22	5.59	32.93	0.977	7.53	14.25	0.81	0.999
	75	10.92	5.48	22.57	0.984	11.36	9.09	1.17	0.999
0.6 g L^{-1}	100	13.98	9.97	33.16	0.909	14.58	7.55	1.60	0.999
	125	17.18	10.28	23.95	0.949	17.92	5.18	1.66	0.999
	150	20.26	11.87	25.33	0.937	21.05	4.84	2.15	0.999
	200	25.87	12.11	20.73	0.963	26.74	4.25	3.04	1.000

as shown in Table 5. We conclude that the correlation coefficients R^2 with high values indicating the applicability of the Elovich kinetic model to the experimental data obtained for adsorption of chromium on Cs/MWCNT/PVA hydrogel.

3.2.4.4. Intraparticle diffusion kinetic model

The equation of the intraparticle diffusion model was first employed in 1988 by Weber and Morris [74] and was given as Eq. (17) [75].

$$q_t = K_{dif}t^{1/2} + C \tag{17}$$

where the intraparticle diffusion rate constant is K_{dif} and C is the intercept of linear line produced when q_t was plotted against $t^{1/2}$ that give important data about the boundary layer thickness, since as the intercept increases the external mass transfer resistance increase also. When plot q_t vs. $t^{1/2}$ we obtain a straight line as shown in Fig. 9d, we can conclude that the linear relationships did not pass through the origin with R^2 of low value. In addition, from Table 5 we note that
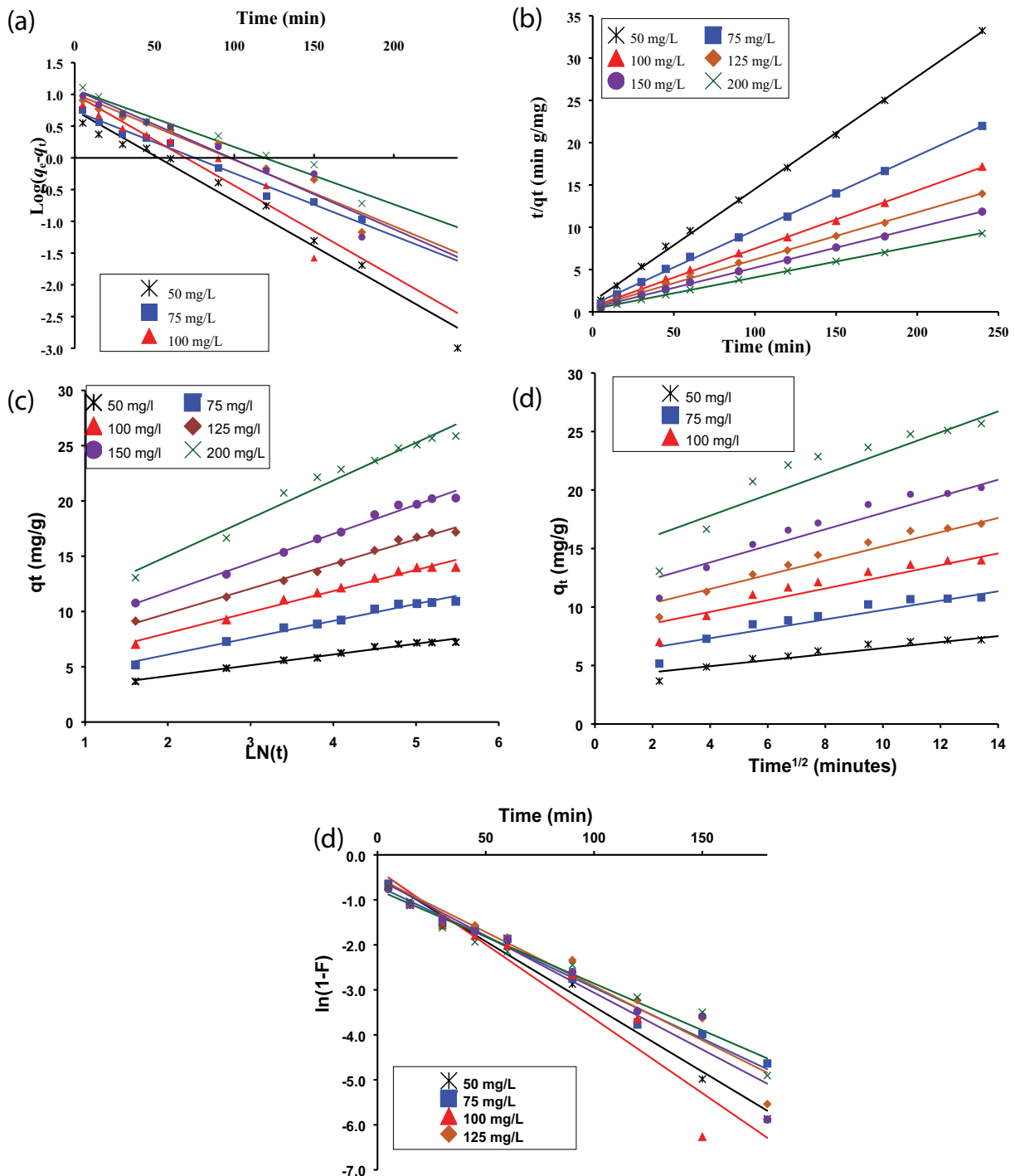
Fig. 9. (a) Pseudo-first-order, (b) pseudo-second-order, (c) Elovich, (d) intraparticle diffusion and (e) film diffusion kinetics of Cr[6+] (50–200 mg L^{−1}) adsorbed onto Cs/MWCNT/PVA hydrogel (0.1–0.6 g L^{−1}) at pH 1.5 and temperature (25°C ± 2°C).

the intercept value increase with increasing of initial chrome concentration meaning that the boundary layer thickness also increased and decrease the external mass transfer at the same time increase the chance of internal mass transfer. In contrast, the *C* value was decreased by increasing the adsorbent dose indicating reducing the thickness of the boundary layer and enhance the external mass transfer. We can conclude the

intraparticle diffusion cannot be the rate-limiting step in the adsorption of chromium on Cs/MWCNT/PVA hydrogel.

3.2.4.5. Film diffusion kinetic model

In 1947 Boyd [76] introduced his kinetic model to explain the process of diffusion for the adsorption of ions from the

Table 5
Comparison of Elovich, intraparticle diffusion and film diffusion kinetic models

Sorbent dose	Cr(IV) conc.	Elovich			Intraparticle diffusion 2			Film diffusion	
		β	α	R^2	K_{dif}	C	R^2	K_{FD}	R^2
0.1 g L^{-1}	50	0.205	315.73	0.939	1.31	28.73	0.850	0.0310	0.780
	75	0.104	48.84	0.974	2.49	32.65	0.829	0.0277	0.890
	100	0.086	97.69	0.986	3.04	44.93	0.860	0.0269	0.860
	125	0.067	81.10	0.985	3.92	51.34	0.860	0.0281	0.930
	150	0.056	89.06	0.974	4.69	60.23	0.843	0.0298	0.920
	200	0.044	112.56	0.976	5.94	46.82	0.835	0.0268	0.880
0.2 g L^{-1}	50	0.413	127.72	0.964	0.63	13.90	0.824	0.0269	0.550
	75	0.263	104.66	0.974	1.00	19.31	0.845	0.0323	0.900
	100	0.179	56.28	0.978	1.46	22.78	0.838	0.0257	0.770
	125	0.144	56.20	0.983	1.84	26.64	0.864	0.0295	0.930
	150	0.118	52.26	0.988	2.24	30.11	0.872	0.0280	0.840
	200	0.100	103.44	0.981	2.63	41.12	0.845	0.0264	0.800
0.3 g L^{-1}	50	0.413	127.72	0.964	0.48	7.63	0.784	0.0264	0.810
	75	0.263	104.66	0.974	0.73	13.19	0.858	0.0296	0.870
	100	0.179	53.54	0.978	0.98	15.22	0.871	0.0294	0.920
	125	0.144	56.20	0.983	1.07	19.81	0.861	0.0283	0.760
	150	0.118	52.26	0.988	1.40	22.87	0.909	0.0274	0.890
	200	0.100	103.44	0.981	1.86	25.27	0.845	0.0249	0.750
0.4 g L^{-1}	50	0.771	36.33	0.961	0.35	6.57	0.853	0.0310	0.880
	75	0.390	13.77	0.944	0.71	8.54	0.900	0.0281	0.940
	100	0.372	40.83	0.971	0.70	12.06	0.834	0.0357	0.860
	125	0.333	85.47	0.969	1.07	19.81	0.861	0.0266	0.680
	150	0.245	37.91	0.992	1.09	16.10	0.892	0.0257	0.850
	200	0.200	55.34	0.983	1.32	20.74	0.861	0.0324	0.940
0.5 g L^{-1}	50	0.953	27.60	0.946	0.27	5.35	0.772	0.0342	0.900
	75	0.594	19.00	0.985	0.45	6.95	0.898	0.0259	0.870
	100	0.524	78.45	0.991	0.51	10.38	0.884	0.0296	0.830
	125	0.360	22.81	0.983	0.73	10.69	0.860	0.0312	0.850
	150	0.326	40.26	0.991	0.82	13.16	0.895	0.0271	0.870
	200	0.235	29.48	0.983	1.11	15.80	0.837	0.0260	0.840
0.6 g L^{-1}	50	1.030	9.58	0.982	0.257	3.911	0.867	0.0290	0.096
	75	0.655	11.23	0.979	0.401	5.73	0.849	0.0283	0.89
	100	0.526	17.75	0.982	0.499	7.585	0.853	0.0364	0.890
	125	0.448	24.64	0.991	0.607	9.114	0.92	0.0283	0.9
	150	0.380	30.96	0.989	0.706	10.99	0.896	0.0297	0.89
	200	0.293	37.40	0.972	0.891	14.24	0.831	0.0272	0.82

aqueous solutions to solid phase and postulated the film diffusion equation as follows.

$$\ln(1-F) = -K_{FD}(t) \tag{18}$$

where ($F = q_t/q_e$) called the fractional attainment of the equilibrium and K_{FD} is the film diffusion constant rate.

By plotting $\ln(1-F)$ vs. time we obtained linear relationship as in Fig. 9e. which did not pass the origin indicating that the film diffusion is not the rate-determining step in the overall adsorption process, this was confirmed by comparison of the absorption correlation coefficient Table 5 ranged from 0.75 to 0.93 which is low values without definite meaning.

4. Conclusion

In this study, a novel tri-dimensional Cs/MWCNT/PVA nanocomposite in the form of hydrogel was successfully prepared with an easier method to be handled. The CVD method used here was a cheap method compared to the others for MWCNT production. The prepared composite has high adsorption capacity and easily removed

from the wastewater after exploitation. The batch experiment indicates that Cs/MWCNT/PVA nanocomposite has a comparable adsorption efficiency for Cr^{6+}. The uptake of the Cr^{6+} was greatly depending on the pH of the solution, proved that chromium ions are best adsorbed at optimum pH 1.5, The kinetics of Cr^{6+} adsorption have poor fit with pseudo-first-order kinetic equation while they have very well-fitting with pseudo-second-order kinetic expression since the correlation coefficient was about unity. The maximum adsorption capacity for the hydrogel was 217.5 mg g^{-1}, which is higher than many reported data in previous literature. The Freundlich isotherm adsorption model having higher R^2 values of 0.96 to 1.0 described the adsorption process better than Langmuir and Temkin models. This novel hydrogel nanocomposite opens new opportunities for different uses of the nanomaterials in various fields of applications in wastewater treatment plants and chemical industries.

References

[1] A. El Nemr, Impact, Monitoring, and Management of Environmental Pollution, Pollution Science, Technology & Abatement Series, Nova Science Publishers Incorporated, , New York, USA 2010.

[2] A. El Nemr, Non-conventional Textile Waste Water Treatment, Nova Science Publishers, New York, USA, 2012.

[3] J. Koropatnick, M. Leibbrandt, Effects of Metals on Gene Expression, Toxicology of Metals, Springer, Berlin, Heidelberg 1995, pp. 93–120.

[4] M. Moncur, C. Ptacek, D. Blowes, J. Jambor, Release, transport and attenuation of metals from an old tailings impoundment, Appl. Geochem., 20 (2005) 639–659.

[5] K. Shekhawat, S. Chatterjee, B. Joshi, Chromium toxicity and its health hazards, Int. J. Adv. Res., 3 (2015) 167–172.

[6] A. El Nemr, Petroleum Contamination in Warm and Cold Marine Environments, Nova Publishers, , New York, USA 2006.

[7] Ihsanullah, F.A. Al-Khaldi, B. Abu-Sharkh, A.M. Abulkibash, M.I. Qureshi, T. Laoui, M.A. Atieh, W. Treatment, Effect of acid modification on adsorption of hexavalent chromium (Cr(VI)) from aqueous solution by activated carbon and carbon nanotubes, Desal. Wat. Treat., 57 (2016) 7232–7244.

[8] C. OEHHA, Air Toxics Hot Spots Program Risk Assessment Guidelines, Part IV: Technical Support Document for Exposure Assessment and Stochastic Analysis, California Office of Environmental Health Hazard Assessment, , USA 2000.

[9] S. Langård, A survey of respiratory symptoms and lung function in ferrochromium and ferrosilicon workers, Int. Arch. Occup. Environ. Health., 46 (1980) 1–9.

[10] J.J. Beaumont, R.M. Sedman, S.D. Reynolds, C.D. Sherman, L.-H. Li, R.A. Howd, M.S. Sandy, L. Zeise, G.V.J.E. Alexeeff, Cancer mortality in a Chinese population exposed to hexavalent chromium in drinking water, Epidemiology, 19 (2008) 12–23.

[11] EPA, Office of Research, W. Development, DC, Toxicological Review of Trivalent Chromium (CAS No. 16065-83-1), 1998.

[12] F.C. Richard, A.C.M. Bourg, Aqueous geochemistry of chromium: a review, Water Res., 25 (1991) 807–816.

[13] R.L. Ramos, A.J. Martinez, R.M.G. Coronado, Adsorption of chromium(VI) from aqueous solutions on activated carbon, Water Sci. Technol., 30 (1994) 191–197.

[14] D. Swami, D. Buddhi, Removal of contaminants from industrial wastewater through various non-conventional technologies: a review, Int. J. Environ. Pollut., 27 (2006) 324–346.

[15] S. Mondal, Methods of dye removal from dye house effluent—an overview, Environ. Eng. Sci., 25 (2008) 383–396.

[16] A. El Nemr, A. El Sikaily, A. Khaled, O. Abdelwahab, Removal of toxic chromium(VI) from aqueous solution by activated carbon using *Casuarina equisetifolia*, Chem. Ecol., 23 (2007) 119–129.

[17] A. El Nemr, A. El-Sikaily, A. Khaled, O. Abdelwahab, Removal of toxic chromium from aqueous solution, wastewater and saline water by marine red alga *Pterocladia capillacea* and its activated carbon, Arabian J. Chem., 8 (2015) 105–117.

[18] A. El Nemr, A. Khaled, O. Abdelwahab, A. El-Sikaily, Treatment of wastewater containing toxic chromium using new activated carbon developed from date palm seed, J. Hazard. Mater., 152 (2008) 263–275.

[19] O. Abdelwahab, A. El Sikaily, A. Khaled, A. El Nemr, Mass-transfer processes of chromium (VI) adsorption onto guava seeds, Chem. Ecol., 23 (2007) 73–85.

[20] A. El Nemr, M.M. El Sadaawy, A. Khaled, A. El Sikaily, Adsorption of the anionic dye Direct Red 23 onto new activated carbons developed from *Cynara cardunculus*: kinetics, equilibrium and thermodynamics, Blue Biotechnol. J., 3 (2014) 121–142.

[21] A. El Nemr, A. El Sikaily, A. Khaled, Modeling of adsorption isotherms of Methylene Blue onto rice husk activated carbon, Egypt. J. Aquat. Res., 36 (2010) 403–425.

[22] Z.A. ALOthman, Mu. Naushad, R. Ali, Kinetic, equilibrium isotherm and thermodynamic studies of Cr(VI) adsorption onto low-cost adsorbent developed from peanut shell activated with phosphoric acid, Environ. Sci. Pollut. Res., 20 (2013) 3351–3365.

[23] M.A. Hashem, M.A. Momen, M. Hasan, M.S. Nur-A-Tomal, M.H. Sheikh, Chromium removal from tannery wastewater using *Syzygium cumini* bark adsorbent, Int. J. Environ. Sci. Technol., 16 (2019) 1395–1404.

[24] S. Bibi, T. Yasin, S. Hassan, M. Riaz, M. Nawaz, Chitosan/CNTs green nanocomposite membrane: synthesis, swelling and poly-aromatic hydrocarbons removal, Mater. Sci. Eng., C, 46 (2015) 359–365.

[25] M. Naushad, Z.A. ALOthman, G. Sharma, Inamuddin, Kinetics, isotherm and thermodynamic investigations for the adsorption of Co(II) ion onto crystal violet modified amberlite IR-120 resin, Ionics, 21 (2015) 1453–1459.

[26] Mu. Naushad, Surfactant assisted nano-composite cation exchanger: development, characterization and applications for the removal of toxic Pb^{2+} from aqueous medium, Chem. Eng. J., 235 (2014) 100–108.

[27] Q. Wan, M. Liu, Y. Xie, J. Tian, Q. Huang, F. Deng, L. Mao, Q. Zhang, X. Zhang, Y. Wei, Facile and highly efficient fabrication of graphene oxide-based polymer nanocomposites through mussel-inspired chemistry and their environmental pollutant removal application, J. Mater. Sci., 52 (2017) 504–518.

[28] E.N. Zare, A. Motahari, M. Sillanpää, Nanoadsorbents based on conducting polymer nanocomposites with main focus on polyaniline and its derivatives for removal of heavy metal ions/dyes: a review, Environ. Res., 162 (2018) 173–195.

[29] B. Pan, X. Zhang, Z. Jiang, Z. Li, Q. Zhang, J. Chen, Polymer and polymer-based nanocomposite adsorbents for water treatment, R. Das, Ed., Polymeric Materials for Clean Water, Springer, Cham, 2019, pp. 93–119.

[30] I. Younes, M. Rinaudo, Chitin and chitosan preparation from marine sources. Structure, properties and applications, Mar. Drugs, 13 (2015) 1133–1174.

[31] K. Kurita, Chitin and chitosan: functional biopolymers from marine crustaceans, Mar. Biotechnol., 8 (2006) 203.

[32] G. Crini, N. Morin-Crini, N. Fatin-Rouge, S. Deon, P. Fievet, Metal removal from aqueous media by polymer-assisted ultrafiltration with chitosan, Arabian J. Chem., 10 (2017) S3826–S3839.

[33] A. Li, R. Lin, C. Lin, B. He, T. Zheng, L. Lu, Y. Cao, An environment-friendly and multi-functional absorbent from chitosan for organic pollutants and heavy metal ion, Carbohydr. Polym., 148 (2016) 272–280.

[34] B. Sarkar, S. Mandal, Y.F. Tsang, P. Kumar, K.-H. Kim, Y.S. Ok, Designer carbon nanotubes for contaminant removal in water and wastewater: a critical review, Sci. Total Environ., 612 (2018) 561–581.

[35] C. Thamaraiselvan, S. Lerman, K. Weinfeld-Cohen, C.G. Dosoretz, Characterization of a support-free carbon nanotube-microporous membrane for water and wastewater filtration, Sep. Purif. Technol., 202 (2018) 1–8.

[36] R. Schmuhl, H. Krieg, K. Keizer, Adsorption of Cu(II) and Cr(VI) ions by chitosan: kinetics and equilibrium studies, Water S.A., 27 (2001) 1–8.

[37] A. El Nemr, Potential of pomegranate husk carbon for Cr(VI) removal from wastewater: kinetic and isotherm studies, J. Hazard. Mater., 161 (2009) 132–141.

[38] N. Sankararamakrishnan, A. Dixit, L. Iyengar, R. Sanghi, Removal of hexavalent chromium using a novel cross linked xanthated chitosan, Bioresour. Technol., 97 (2006) 2377–2382.

[39] Y. Liu, J. Wang, Y. Zheng, A. Wang, Adsorption of methylene blue by kapok fiber treated by sodium chlorite optimized with response surface methodology, Chem. Eng. J., 184 (2012) 248–255.

[40] G. Sharma, M. Naushad, A.H. Al-Muhtaseb, A. Kumar, M.R. Khan, S. Kalia, Shweta, M. Bala, A. Sharma, Fabrication and characterization of chitosan-crosslinked-poly(alginic acid) nanohydrogel for adsorptive removal of Cr(VI) metal ion from aqueous medium, Int. J. Biol. Macromol., 95 (2017) 484–493.

[41] A. El-Sikaily, A. El Nemr, A. Khaled, O. Abdelwehab, Removal of toxic chromium from wastewater using green alga *Ulva lactuca* and its activated carbon, J. Hazard. Mater., 148 (2007) 216–228.

[42] J.A. Schwarz, C. Contescu, A. Contescu, Methods for preparation of catalytic materials, Chem. Rev., 95 (1995) 477–510.

[43] M. Bahgat, A. Farghali, W. El Rouby, M. Khedr, Synthesis and modification of multi-walled carbon nano-tubes (MWCNTs) for water treatment applications, J. Anal. Appl. Pyrolysis., 92 (2011) 307–313.

[44] A.A. Alqadami, Mu. Naushad, Z.A. Alothman, A.A. Ghfar, Novel metal–organic framework (MOF) based composite material for the sequestration of U(VI) and Th(IV) metal ions from aqueous environment, ACS Appl. Mater. Interfaces, 9 (2017) 36026–36037.

[45] V.A. Pereira, I.N.Q. de Arruda, R. Stefani, Active chitosan/PVA films with anthocyanins from *Brassica oleraceae* (Red Cabbage) as time–temperature indicators for application in intelligent food packaging, Food Hydrocolloids, 43 (2015) 180–188.

[46] Z. Yu, B. Li, J. Chu, P. Zhang, Silica in situ enhanced PVA/chitosan biodegradable films for food packages, Carbohydr. Polym., 184 (2018) 214–220.

[47] M. Abbasi, Synthesis and characterization of magnetic nano-composite of chitosan/SiO$_2$/carbon nanotubes and its application for dyes removal, J. Cleaner Prod., 145 (2017) 105–113.

[48] M. Hui, P. Shengyan, H. Yaqi, Z. Rongxin, Z. Anatoly, C. Wei, A highly efficient magnetic chitosan "fluid" adsorbent with a high capacity and fast adsorption kinetics for dyeing wastewater purification, Chem. Eng. J., 345 (2018) 556–565.

[49] A.A. Alqadami, Mu. Naushad, M.A. Abdalla, M.R. Khan, Z.A. Alothman, Adsorptive removal of toxic dye using Fe$_3$O$_4$–TSC nanocomposite: equilibrium, kinetic, and thermodynamic studies, J. Chem. Eng. Data, 16 (2016) 3806–3813.

[50] A. Zanotto, A. Luyt, A. Spinella, E. Caponetti, Improvement of interaction in and properties of PMMA-MWNT nanocomposites through microwave assisted acid treatment of MWNT, Eur. Polym. J., 49 (2013) 61–69.

[51] M. Steimecke, S. Ruemmler, M. Bron, The effect of rapid functionalization on the structural and electrochemical properties of high-purity carbon nanotubes, Electrochim. Acta, 163 (2015) 1–8.

[52] H. Sadegh, R. Shahryari-ghoshekandi, S. Agarwal, I. Tyagi, M. Asif, V.K. Gupta, Microwave-assisted removal of malachite green by carboxylate functionalized multi-walled carbon nanotubes: kinetics and equilibrium study, J. Mol. Liq., 206 (2015) 151–158.

[53] S. Mor, K. Ravindra, N.R. Bishnoi, Adsorption of chromium from aqueous solution by activated alumina and activated charcoal, Bioresour. Technol., 98 (2007) 954–957.

[54] Y.G. Ko, U.S. Choi, T.Y. Kim, D.J. Ahn, Y.J. Chun, FT-IR and isotherm study on anion adsorption onto novel chelating fibers, Macromol. Rapid Commun., 23 (2002) 535–539.

[55] F. Gode, E. Pehlivan, Removal of Cr(VI) from aqueous solution by two Lewatit-anion exchange resins, J. Hazard. Mater., 119 (2005) 175–182.

[56] E. Demirbas, M. Kobya, E. Senturk, T. Ozkan, Adsorption kinetics for the removal of chromium(VI) from aqueous solutions on the activated carbons prepared from agricultural wastes, Water SA, 30 (2004) 533–539.

[57] E. Malkoc, Y. Nuhoglu, The removal of chromium(VI) from synthetic wastewater by *Ulothrix zonata*, Fresenius Environ. Bull., 12 (2003) 376–381.

[58] Z. Holan, B. Volesky, I. Prasetyo, Biosorption of cadmium by biomass of marine algae, Biotechnol. Bioeng., 41 (1993) 819–825.

[59] A. Mittala, Mu. Naushad, G. Sharma, Z.A. ALothmanb, S.M. Wabaidur, M. Alam, Fabrication of MWCNTs/ThO$_2$ nanocomposite and its adsorption behaviorfor the removal of Pb(II) metal from aqueous medium, Desal. Wat. Treat., 57 (2016) 21863–21869.

[60] E. Longhinotti, F. Pozza, L. Furlan, M. Sanchez, M. Klug, M. Laranjeira, T. Fávere, Adsorption of anionic dyes on the biopolymer chitin, J. Braz. Chem. Soc., 9 (1998) 435–440.

[61] Mu. Naushad, G. Sharma, A. Kumar, S. Sharma, A.A. Ghfar, A. Bhatnagar, F.J. Stadler, M.R. Khan, Efficient removal of toxic phosphate anions from aqueous environment using pectin based quaternary amino anion exchanger, Int. J. Biol. Macromol., 106 (2018) 1–10.

[62] H. Freundlich, Uber die adsorption in losungen, zeitschrift fur phtsikalische chemie, Am. Chem. Soc., 62 (1906) 121–125.

[63] G. Crini, H.N. Peindy, F. Gimbert, C. Robert, Removal of CI Basic Green 4 (Malachite Green) from aqueous solutions by adsorption using cyclodextrin-based adsorbent: kinetic and equilibrium studies, Sep. Purif. Technol., 53 (2007) 97–110.

[64] L. Yanyan, T.A. Kurniawan, A.B. Albadarin, G. Walker, Enhanced removal of acetaminophen from synthetic wastewater using multi-walled carbon nanotubes (MWCNTs) chemically modified with NaOH, HNO$_3$/H$_2$SO$_4$, ozone, and/or chitosan, J. Mol. Liq., 251 (2018) 369–377.

[65] M. Temkin, V. Pyzhev, Kinetics of ammonia synthesis on promoted iron catalyst, Acta Physiochim. URSS, 12 (1940) 327–356.

[66] F. Wang, L.-Y. Liu, F. Liu, L.-G. Wang, T. Ouyang, C.-T. Chang, Facile one-step synthesis of magnetically modified biochar with enhanced removal capacity for hexavalent chromium from aqueous solution, J. Taiwan Inst. Chem. Eng., 81 (2017) 414–418.

[67] G. Akkaya, A. Özer, Biosorption of Acid Red 274 (AR 274) on *Dicranella varia*: determination of equilibrium and kinetic model parameters, Process Biochem., 40 (2005) 3559–3568.

[68] A. Farhan, K. Ong, W.W. Yunus, M. Jabit, A. Fitrianto, A. Hussin, A. Sulaiman, S. Jamal, J. Osman, C.C. Teoh, Kinetics study of nickel(II) ions sorption by thermally treated rice husk, Nat. Environ. Pollut. Technol., 16 (2017) 889–892.

[69] S.H. Lagergren, Zur theorie der sogenannten adsorption geloster stoffe, K. Sven. Vetenskapsakad. Handl., 24 (1898) 1–39.

[70] Y. Ho, G. McKay, D. Wase, C.F. Forster, Study of the sorption of divalent metal ions on to peat, Adsorpt. Sci. Technol., 18 (2000) 639–650.

[71] J. Zeldowitsch, Über den mechanismus der katalytischen oxidation von CO and MnO$_2$, Acta Physicochim. URSS, 1 (1934) 364–449.

[72] S.H. Chien, W.R. Clayton, Application of Elovich equation to the kinetics of phosphate release and sorption on soils, Soil Sci. Soc. Am. J., 44 (1980) 265–268.

[73] D.L. Sparks, Kinetics of Reaction in Pure and Mixed Systems, Soil Physical Chemistry, CRC Press, Boca Raton, 1986.

[74] W.J. Weber, J.C. Morris, Kinetics of adsorption on carbon from solution, J. Sanit. Eng. Div. Am. Soc. Civ. Eng., 89 (1963) 31–60.

[75] J.P. Simonin, J. Boute, Intraparticle diffusion-adsorption model to describe liquid/solid adsorption kinetics, Revista Mexicana de Ingeniería Química, 15 (2016) 161–173.

[76] G.E. Boyd, A.M. Adamson, L.S. Myers, The exchange adsorption of ions from aqueous solutions by organic zeolites, J. Am. Chem. Soc., 69 (1947) 2836.